Published in final edited form as:
Exp Gerontol. 2012 April ; 47(4): 304–316. doi:10.1016/j.exger.2012.01.004.

Endogenously Determined Restriction of Food Intake Overcomes Excitation-Contraction Uncoupling in JP45KO Mice with Aging

Osvaldo Delbono[1], **Maria Laura Messi**[1], **Zhong-Min Wang**[1], **Susan Treves**[4], **Barbara Mosca**[6], **Leda Bergamelli**[6], **Miyuki Nishi**[5], **Hiroshi Takeshima**[5], **Hang Shi**[1,3], **Bingzhong Xue**[2,3], and **Francesco Zorzato**[4,6]

[1]Department of Internal Medicine, Section on Gerontology and Geriatric Medicine, Wake Forest University School of Medicine, Winston-Salem, NC 27157 [2]Section on Endocrinology and Metabolism, Wake Forest University School of Medicine, Winston-Salem, NC 27157 [3]Center of Diabetes Research, Wake Forest University School of Medicine, Winston-Salem, NC 27157 [4]Departments of Anaesthesia and Research, Basel University Hospital, Hebelstrasse 20, 4031 Basel, Switzerland [5]Department of Biological Chemistry, Graduate School of Pharmaceutical Sciences, Kyoto University, Kyoto 606-8501, Japan [6]Department of Experimental and Diagnostic Medicine, General Pathology Section, University of Ferrara, Via Borsari 46, 44100 Ferrara, Italy

Abstract

The decline in muscular strength with age is disproportionate to the loss in total muscle mass that causes it. Knocking out JP45, an integral protein of the junctional face membrane of the skeletal muscle sarcoplasmic reticulum (SR), results in decreased expression of the voltage-gated Ca^{2+} channel, $Ca_V1.1$; excitation-contraction uncoupling (ECU); and loss of muscle force (Delbono et al., 2007). Here, we show that $Ca_V1.1$ expression, charge movement, SR Ca^{2+} release, in vitro contractile force, and sustained forced running remain stable in male JP45KO mice at 12 and 18 months. They also exhibit the level of ECU reported for 3–4-month mice (Delbono et al., 2007). No further decline at later ages was recorded. Preserved ECC was not related to increased expression of any protein that directly or indirectly interacts with JP45 at the triad junction. However, maintained muscle force and physical performance were associated with ablation of JP45 expression in the brain, spontaneous and significantly diminished food intake and less tendency toward obesity when exposed to a high-fat diet compared to WT. We propose that (1) endogenously generated restriction in food intake overcomes the deleterious effects of JP45 ablation on ECC and skeletal muscle force mainly through downregulation of neuropeptide-Y expression in the hypothalamic arcuate nucleus; and (2) the JP45KO mouse constitutes an invaluable model to examine the mechanisms controlling food intake as well as skeletal muscle function with aging.

Address correspondence to: Osvaldo Delbono, MD, PhD., Wake Forest University School of Medicine, 1 Medical Center Boulevard, Winston-Salem, NC 27157, Phone: (336)716-9802, Fax: (336)716-2273, odelbono@wfubmc.edu.

Keywords

Skeletal muscle; aging; JP45; excitation-contraction uncoupling; food intake; caloric restriction

1. INTRODUCTION

Skeletal muscle contraction in response to muscle fiber excitation (sarcolemmal depolarization), termed *excitation-contraction coupling* (ECC), is mediated by a transient elevation in intracellular Ca^{2+} concentration (Melzer et al., 1995). ECC starts at the triad junction, a structure where the transverse (T) tubule and the sarcoplasmic reticulum (SR) terminal cisternae intimately interact via the two major Ca^{2+} channel macromolecular complexes interact, the voltage-gated Ca^{2+} channel $Ca_v1.1$, previously known as DHPRα_{1S} (Catterall et al., 2005), containing both the Ca^{2+}-conducting pore and the voltage-sensing S4 domain, which is localized in the transverse (T) tubule membranes, and the ryanodine receptor (RyR) Ca^{2+}-release channel localized in the SR terminal cisternae. The Ca_v1 is a hetero-oligomeric complex made up of at least four subunits: $Ca_v1.1$, β1a, α2-δ and γ (Catterall, 1995) and the pore-forming $Ca_v1.1$ subunit is an integral membrane protein and essential for ECC (Melzer et al., 1995). The close proximity of the $Ca_v1.1$ and RyR1 allows sarcolemmal depolarization to rapidly (within ms) translate into SR Ca^{2+} release, prompting formation of contractile myofilament cross-bridges and generating force.

The decline in muscular strength with age is disproportionate to the loss in total muscle mass that largely causes it. This loss of specific force (total force/cross-sectional area) in old age (Gonzalez et al., 2000a) is characterized, in part, by a deficit in Ca^{2+} release following depolarization, a phenomenon known as *excitation-contraction uncoupling (ECU)* (Jimenez-Moreno et al., 2008). We have proposed that ECU is not a result of decreased Ca^{2+} stores or RyR1-mediated release function (Jimenez-Moreno et al., 2008) but may be caused by alterations in the functionality and expression of Ca_v1 and its subunits with aging (Renganathan et al., 1997a; Taylor et al., 2009).

A variety of proteins with a putative role in ECC are found at the triad. Our previous studies demonstrated that JP45, a protein integral to the skeletal muscle SR junctional face membrane, interacts with $Ca_v1.1$ and the luminal Ca^{2+}-binding protein, calsequestrin (Anderson et al., 2006; Delbono et al., 2007). $Ca_v1.1$ and JP45 form a complex that is downregulated during aging and may contribute to decayed muscle strength and physical disability in the elderly (Anderson et al., 2006; Wang et al., 2000). Deleting the gene that encodes JP45 results in decreased muscle strength in young mice due to decreased functional expression of the voltage-dependent Ca^{2+} channel $Ca_v1.1$ (Delbono et al., 2007).

These results underscore the importance of JP45 as a molecule involved in the development and maintenance of skeletal muscle strength throughout life. To test this concept, we examined ECC in 12- and 18-month-old JP45 knockout (KO) and wild-type (WT) mice. We hypothesized that ablation of JP45 expression together with diminished $Ca_v1.1$ expression would result in more marked muscle weakness in JP45KO than WT mice with aging. Surprisingly, aging male JP45KO mice exhibit less food intake and significantly lower trend to develop obesity than WT mice when exposed to high-fat diet. As caloric restriction is a powerful antiaging intervention (Mayhew et al., 1998)(Marzetti et al., 2008)(Sakuma and Yamaguchi, 2010), we reasoned that it mediates protective effects on skeletal muscle protein expression and function in JP45KO mice with aging. Here, we postulate that self-imposed or endogenously developed restriction of food intake accounts for their sustained muscle force, response to highly demanding exercise, and $Ca_v1.1$ expression. We also found that the JP45KO mouse is a model of endogenous, moderate, sustained restriction of food intake, not

associated with disease or hibernation. We propose that an imbalance in orexigenic and anorexigenic hypothalamic neuropeptide secretion leads to reduced food consumption and a lean phenotype. This mouse model may prove invaluable in examining the mechanisms controlling food intake and preserving skeletal muscle function with aging.

2. MATERIAL AND METHODS

2.1 . Flexor digitorum brevis, soleus and flexor digitorum brevis muscle fibers

Extensor digitorum longus (EDL) and *soleus* muscles and single *flexor digitorum brevis* (FDB) fibers were obtained from 12- and 18-month male JP45KO and C57BL6 (WT) mice raised in the Wake Forest University School of Medicine (WFUSM) Animal Research Program. Mice subjected to activity recording and/or training did not participate in more than one experiment. They were killed by cervical dislocation and thoroughly inspected for gross pathology. Animal handling followed a protocol approved by the WFUSM Animal Care and Use Committee.

2.2. Generation of JP45KO Mice

JP45KO mice were generated as previously described (27). Briefly, a mouse genomic library (Stratagene) was screened with a cDNA probe to isolate genomic clones encompassing the 5′ end of the JP45 gene. A targeting vector was constructed using a 5′-end JP45 genomic clone, neo-resistance, and the diphtheria toxin gene DT-A as positive and negative selection cassettes, respectively. A SalI-linearized vector was used to transfect J1 mouse embryonic stem (ES) cells, and 140 ES clones carrying a homologous recombination were identified by Southern blot screening. JP45−/− mice were backcrossed three times in a C57BL6 background and then intercrossed to obtain JP45−/− mice. Genotyping was carried out by PCR using the following primers: JP45F2, 5′-TAA AGA CAG AGA CCA CAT CCT CCC-3′; JP45R4, 5′-GAC AAG GGG TGT GGG GTA TGA GGC-3′ (Delbono et al., 2007).

2.3. In vitro muscle force assessment

EDL and soleus muscles were stimulated directly by an electrical field generated between two parallel platinum electrodes connected to a stimulator (Heidelberg Scientific Instruments, Heidelberg, Germany or Grass S48, Warwick, RI). Muscle length was adjusted to the estimate of sarcomere length eliciting maximal twitch and tetanic force (L_o). Rectangular supramaximal pulses (1.5x threshold and 0.5 ms duration) were applied to elicit brief contractions. Trains of pulses of variable frequency, ranging from 10 to 150Hz, were applied for 400 ms (EDL) or 1100 ms (soleus) to elicit unfused or fused contractions. All the experiments were performed at room temperature (21–23°C). The solution used for contraction recording contained (mM): NaCl 121, KCl 5, $CaCl_2$ 1.8, $MgCl_2$ 0.5, NaH_2PO_4 0.4, $NaHCO_3$ 24.0, glucose 5.5, and EDTA 0.1. It was permanently bubbled with a mixture of 5% CO_2 and 95% O_2 to attain pH 7.4 in the recording chamber. The interval between trains of pulses was constant (5 min). Force recordings were digitized using an A/D converter (AD Instruments) at 4 kHz. Stimulation pulse waveform was acquired and digitized together with the contraction signal and stored for analysis off-line. Specific force was normalized to the muscle cross-sectional area (CSA= wet weight [mg]/length [mm] x 1.06 [density mg/mm^3]). Muscle length was measured in the recording chamber at L_o by stereoscopic visualization at 30X magnification.

2.4. Charge-movement recordings

FDB fibers from JP45KO and WT mice were enzymatically dissociated, plated, and recorded as previously described (Wang et al., 1999a). For the whole-cell patch clamp, the pipette solution was 140 mM Cs-aspartate, 5 mM Mg-$aspartate_2$, 10 mM Cs2EGTA

[ethylene glycol-bis(α-aminoethyl ether)-*N*,*N*,*N*′*N*′-tetraacetic acid], and 10 mM Hepes [*N*-(2-hydroxyethyl)piperazine-*N*′-(2-ethanesulfonic acid)]. The pH was adjusted to 7.4 with CsOH. The external solution contained (mM): 145 tetraethylammonium hydroxide (TEA). Cl, 10 $CaCl_2$, 10 Hepes, and 0.001 tetrodotoxin. Solution pH was adjusted to 7.4 with TEA.OH. For charge-movement recording, Ca^{2+} current was blocked by adding 0.5 Cd^{2+} plus 0.3 La^{3+} to the external solution (Adams et al., 1990; Wang et al., 2000). We recorded $Ca_v1.1$ channel charge movement using a protocol consisting of a 2-s prepulse to −30 mV and a subsequent 5-ms repolarization to a pedestal potential of −50 mV followed by a 25-ms depolarization from −50 mV to 50 mV with 10-mV intervals (Anderson et al., 2006). Intramembrane charge movements were calculated as the integral of the current in response to depolarizing pulses and expressed per membrane capacitance (coulombs per farad). To analyze the relationship between charge movement and membrane voltage, data points were fitted to equation 1.

2.5. Sarcoplasmic reticulum Ca^{2+} release

Enzymatically dissociated fibers were transferred to a small, flow-through Lucite chamber positioned on a microscope stage and continuously perfused with the external solution (see below) using a push-pull syringe pump (WPI). Only fibers exhibiting a clean surface and no contracture were used for electrophysiological recordings. Muscle fibers were voltage-clamped using an Axopatch-200B amplifier (Molecular Devices) in the whole-cell configuration of the patch-clamp technique (Hamill et al., 1981). Patch pipettes were pulled from borosilicate glass (Boralex; WPI, Sarasota, FL) using a Flaming Brown micropipette puller (P97, Sutter Instrument Co., Novato, CA) then fire-polished to obtain electrode resistances ranging from 450 to 650 kΩ. In the cell-attached configuration, the seal resistance was in the range of 1–4.5 GΩ, and in the whole-cell configuration, values ranged from 75 to 120 MΩ (Wang et al., 1999a).

The pipette was filled with the following solution (mM): 140 Cs-aspartate, 5 $Mgaspartate_2$, 20 Cs_2EGTA (ethylene glycol tetraacetic acid), 10 HEPES (N-[2-hydroxyethyl]piperazine-N′-[2-ethanesulfonic acid]), and 500 OGB-5N (Invitrogen, Carlsbad, CA), and pH was adjusted to 7.4 with CsOH (Adams et al., 1990; Wang et al., 1999a). The external solution contained (mM): 150 TEA-CH_3SO_3, 2 $MgCl_2$, 2 $CaCl_2$, 10 Na-HEPES, 0.05 N-benzyl-p-toluene sulphonamide (BTS), and 0.001 tetrodotoxin (Delbono et al., 1997). Solution pH was adjusted to 7.4 with CsOH. All the experiments were conducted at room temperature (21–22°C).

We used OGB-5N for these experiments due to its high quantum yield and suitability for cell imaging with laser confocal microscopy. The fibers were loaded with it via the patch pipette, and it was allowed to diffuse for 20 to 30 min before fiber stimulation and after attaining the whole-cell voltage-clamp configuration. Intracellular OGB-5N transients were recorded using a Bio-Rad Radiance 2100 laser scanning confocal microscope (Zeiss, Oberkochen, Germany). Confocal microscopy allowed us to improve the signal-noise ratio under experimental conditions in which myoplasmic Ca^{2+} concentration was strongly buffered by 20 mM EGTA to ensure a resting myoplasmic Ca^{2+} concentration value that approached the 60 nM in the pipette (Woods et al., 2004). This experimental manipulation also ensured more accurate estimation of the Ca^{2+} release flux.

Fibers were imaged through a C-Apochromat x 40 water-immersion objective (NA 1.2, Zeiss) or a x20 Fluar (NA 0.75) using a krypton-argon laser at 488-nm excitation wavelength. Fluorescence emission was measured at 528 ± 25nm wavelength. For most experiments, the laser was attenuated to 6–12% with a neutral density filter. Fibers were imaged in line-scan (*x*-*t*) mode, always oriented parallel to the *x* scan direction. Linescan images were acquired with 256 pixels (0.236 μm per pixel) in the *x*- and 512 pixels

(0.833ms per pixel) in the *t*-direction. For image acquisition and intensity profile analysis, we used LaserSharp 2000 (Bio-Rad, Zeiss) and Image- J (NIH), respectively.

2.6. In vivo mouse spontaneous and forced activity

Animals were housed individually in cages equipped with a running wheel carrying a magnet. Wheel revolutions were registered by a reed sensor connected to an I-7053D Digital-Input module (Spectra), and the revolution counters were read by a standard laptop computer via an I-7520 RS-485-to-RS-232 interface converter (Spectra). Digitized signals were processed by the "mouse running" software developed by Santhera Pharmaceuticals.

Forced activity was measured using an Exer 6 lane treadmill (Columbus Instruments, Columbus, OH). Training was as follows. On consecutive days, mice were allowed to run on the treadmill for 5 min at 10 m/min on days 1 and 2 and 5 min at 10 m/min followed by 2 m/min increments until reaching 20 m/min for 2 min each period on day 3. The treadmill was not inclined for the first two days but tilted 5 degrees uphill on the third day. After training, mouse running time was recorded. The initial speed was 10m/min to a maximum of 5 min, and then we increased the pace by 2 m/min every 2 min to a maximum of 24 m/min or until exhaustion. We considered the mouse exhausted when it remained at least 10 sec in the electric shock area of the treadmill. In all cases, the ramp was tilted 5 degrees uphill. Maximal running time sums all partial times at various paces. For instance, a mouse's maximal running time of 9 min indicates that he ran 5 min at 10 m/min plus 2 min at 12 m/min plus 2 min at 14 m/min and did not reach 16, 18, 20, 22, and 24 m/min. If he reached the highest speed (24 m/min), he was allowed to run with no time limit until exhaustion.

2.7. Microsomal preparation, SR protein composition, and [^{3}H]PN200-110 radioligand binding assay

SR membrane fraction isolation (Saito et al., 1984) and SDS/PAGE analysis were carried out as described (Anderson et al., 2006). [^{3}H] PN200-110 and [^{3}H]ryanodine binding was carried out as described (Delbono et al., 2007). Densitometry of the immunopositive bands used BioRad GelDoc 2000. Curve fitting used Prism4 software (GraphPad). Densitometry was analyzed with NIH ImageJ software. For Western blot analysis of SR proteins, we used anti-SERCA1 and - SERCA2 Abs (Santa Cruz Biotechnology, Santa Cruz, CA), anti-RyR1, antisarcalumenin, and anticalreticulin Abs (Thermo Scientific, Waltham, MA). The anticalsequestrin1 and antiJP45 Abs were developed by our group (Anderson et al., 2003). Protein levels were normalized and expressed as percent of albumin, which was immunodetected using the specific antibody A90-134P (Bethyl Laboratories, Montgomery, TX).

2.8. Fiber-type composition and fiber measurement

EDL and soleus muscles were embedded in OCT, snap-frozen in isopentane, cryosectioned at the midbelly region (10μm), and mounted on coverslips for immunostaining. Mounted sections were air-dried, treated with PBS containing 1% BSA and 2% horse serum for 30 min, and incubated overnight at 4–8°C with a PBS solution containing 0.01% Triton X100, 1% BSA, 2% horse serum, 0.5% μg/ml antimouse slow myosin heavy chain (MAB 1628, Millipore, Billerica, MA), and 2 μg/ml antirat α-laminin (MAB1914, Millipore). Sections were then washed with PBS four times for 15 min each and incubated at room temperature for 40 min with a PBS-containing Alexa Fluor 488 antimouse IgG Ab (2 μg/ml) and Cy3 antirat IgG Ab (0.5 μg/ml). After incubation in the secondary Ab, sections were washed with PBS four times for 15 min each, dehydrated with ethanol, and mounted using a glycerol medium at room temperature. They were then imaged using a Leica DM5000B fluorescence microscope. Muscle fiber analysis (Soft Imaging System, Muenster, Germany) determined: (1) boundaries, using laminin immunofluorescence; (2) diameter, using the minimal Feret's

diameter (distance between parallel tangents at opposing borders); (3) percent positive to anti-MHC IAb; and (4) percent negative to anti-MHC I Ab staining.

2.9. Insulin and leptin determinations

Serum insulin and leptin levels were measured using rat insulin enzyme-linked immunosorbent assay (ELISA) and mouse leptin ELISA kits (Crystal Chem, Downers Grove, IL), respectively (Shi et al., 2006).

2.10. Mouse brain immunocytochemistry

JP45 and WT mice were deeply anesthetized with ketamine (200 mg/kg weight) and xylazine (10 mg/kg) and perfused first with 15 ml normal saline and then 10 ml 4% PFA in 0.1 M sodium phosphate buffer (PB) at pH: 7.4 through left ventricle, following published procedures (Hu et al., 2009). The brain was dissected and immersed in the 4% PFA buffer for 24 h at 4°C and then exchanged with fresh PFA and left for another 24h. The brain was rinsed in 10% sucrose in 0.1 M PB for 24h and then in 20% for another day. It was then positioned in an embedding mold, covered with tissue freezing medium TBS (Triangle Biomedical Sciences, Durham, NC), and frozen in dry ice. Coronal sections (40 μm) were obtained using a Leica (Bannockburn, IL) cryostat. Brain sections were dried at room temperature and stored at −80°C. Slides containing various brain slices were rinsed in 4% PFA for 15 min at room temperature and washed three times with PBS, permeabilized in 0.5% triton and 1% goat serum in PBS for 15 min at room temperature, followed by three washes with PBS and blocked in 10% goat serum at 4°C overnight. Slides were rinsed with PBS and incubated in JP45 antibody for 4 h and then exposed to the secondary goat anti-rabbit Alexa Fluor 594 antibody (Invitrogen). Preparations were mounted using Dako (Carpinteria, CA) mounting medium and examined with an IX81 Olympus microscope controlled by Olympus MetaMorph.

2.11. Dissection of hypothalamic regions

Hypothalamic regions were dissected as previously described (Xue et al., 2009). Briefly, each hypothalamic region was dissected from 1-mm-thick sagittal sections of fresh mouse brain. Arcuate (ARH) and paraventricular (PVN) hypothalamus were dissected from the first sections from the midline of the brain. Coordinates for each hypothalamic region were described previously (Xue et al., 2009).

2.12. Quantitative Real-time RT-PCR

Total RNA was isolated from hypothalamus using Tri-Reagent according to the manufacturer's instructions (Molecular Research Center, Cincinnati, OH). Messenger RNAs of specific genes were quantified by real-time RT-PCR using TaqMan One-step RT-PCR Master Mix (Applied Biosystems) and a Stratagene Mx3000P system (Stratagene, La Jolla, CA). The sequences for each primer/probe set are included in Table 1.

2.13. Statistical analysis

Data are presented as means ± S.E.M. and were analyzed with *Student* t-test, Mann-Whitney rank sum test, or one- or two-way repeated measures ANOVA when appropriate. An alpha value of $P < 0.05$ was considered significant.

3. RESULTS

3.1. Mechanical properties of EDL and soleus muscles from 12- and 18-month JP45KO and WT mice

Previous work from our laboratory demonstrated that ablating the SR protein JP45 leads to loss of absolute and specific skeletal muscle force in young (3–4-month) mice (Delbono et al., 2007) (Fig. 1A). Here, we report that the difference in tetanic force between 12-month JP45KO and WT mice is significant only for extensor digitorum longus (EDL), and that all mechanical properties recorded at 18-month JP45KO and WT mice do not differ significantly (Fig. 1A). Changes in the force-frequency curve do not account for their similar force response to brief and tetanic stimulation; a wide range of frequencies were tested per muscle (10, 20, 40, 100, 120, and 150Hz), and the maximal force output was recorded at the same frequency, 150 and 100 Hz for EDL and soleus muscles, respectively, regardless of genetic background or age.

Muscle weight between JP45KO and WT mice at 12 and 18 months of age did not differ significantly. Values expressed in mg, as mean ± SD, were: EDL WT 12 months = 14 ± 1.5; EDL WT 18 = 13 ± 1.2; soleus WT 12 = 10 ± 1.7; soleus WT 18 = 11 ± 1.5; EDL JP45KO 12 = 14 ± 1.7; EDL JP45KO 18 = 13 ± 1.3; soleus JP45KO 12 = 10 ± 1.3; and soleus JP45KO 18 = 11 ± 1.4.

These results support the concept that the difference in muscle force between 3–4-month JP45KO and WT disappears with aging. Since deleting the gene encoding JP45 decreases muscle strength in young mice by diminishing functional expression of the voltage-dependent Ca^{2+} channel $Ca_v1.1$ (Delbono et al., 2007), we examined the functional and biochemical expression of this subunit in 12- and 18-month JP45KO and WT mice.

3.2. $Ca_v1.1$ charge movement and content in total SR membrane from JP45 KO and WT mice

Charge movement, which represents functional expression of $Ca_v1.1$ in the T tubule, was recorded in flexor digitorum brevis (FDB) fibers in the whole-cell configuration of patch-clamp (Hamill et al., 1981; Wang et al., 2000). Although in vitro muscle force was recorded in EDL and soleus muscles, charge movement was recorded in FDB muscle because its short fibers allow voltage-clamping in the whole-cell configuration and undergo age-dependent changes similar to those described for longer hindlimb muscles (Gonzalez et al., 2000a).

The current recorded after blocking the Ca^{2+} current is the intramembrane charge movement. Saturated at both extremes of the voltage range, the amount of charge moved during depolarization (Q_{on}) is equal to the charge that returns during repolarization (Q_{off}), which has been demonstrated for adult skeletal muscle fibers recorded in the whole-cell configuration of the patch-clamp technique (Wang et al., 1999a). We used a protocol consisting of a 2-s prepulse to −30 mV and a subsequent 5-ms repolarization to a pedestal potential of −50-mV, followed by a 25-ms depolarization from −50 to 50-mV with 10-mV intervals (Adams et al., 1990). The membrane potential was held at -80 mV between pulses. The optimal duration of the prepulse is defined as the value at which charge immobilization ceases, or 2s after testing a range of prepulses from 1 to 6-s. Figure 1B shows $Ca_v1.1$ charge movement for 3-, 12- and 18-month JP45KO and WT mice. To analyze the voltage-dependence of the charge, data points were fitted to a Boltzmann equation of the form:

$$Q_{on}=Q_{max}/[1+\exp(V_{1/2Q}-V_m)/K], \quad \text{equation 1}$$

where Q_{max} is the maximal charge; V_m is the membrane potential; $V_{1/2Q}$ is the charge movement half-activation potential; and *K* is the steepness of the curve. Table 2 includes the best-fitting parameters for Q_{max}, $V_{1/2Q}$, and *K*. Values significantly differed for 3- and 12- but not 18-month mice, consistent with the in vitro contraction results reported above.

To determine whether the lack of difference in charge movement results in similar intracellular Ca^{2+} mobilization, we recorded SR Ca^{2+} release. Single FDB fibers were loaded with Oregon-green-bapta-5N (OGB-5N) via the patch pipette, and intracellular Ca^{2+} was recorded using a confocal microscope in the line-scan mode.

To determine the voltage-dependence of intracellular Ca^{2+} release, we applied 40-ms depolarizing voltage steps from the holding potential (−80 mV) to command potentials ranging from −60 to 80 mV. Data points were fitted to a Boltzmann equation of the form:

$$F=F_{max}/[1+\exp(V_{1/2F}-V_m)/K], \quad \text{equation 2}$$

where F_{max} is the maximum charge; and $V_{1/2F}$ is the Ca^{2+} fluorescence half-activation potential. Table 2 shows the best fitting parameters for F_{max},$V_{1/2F}$, and K recorded in muscle fibers from 3-, 12- and 18-month JP45KO and WT mice. No statistically significant difference in SR Ca^{2+} release was recorded between 12-month JP45KO and WT mice, indicating that the significantly different charge movement recorded is not sufficient to compromise intracellular Ca^{2+} mobilization and its voltage-dependent activation. The lack of difference in SR Ca^{2+} release correlates with the similar charge movement recorded in 18-month mice (Fig. 1B).

$Ca_v1.1$ content was assessed by radioligand-binding assay and normalized to albumin content in muscle SR fraction (Fig. 1C). Maximal [^{3}H]-PN200-110 binding number did not differ significantly between 18-month JP45KO and WT mice. Albumin was measured by densitometry of the protein band detected with an albumin antibody and used as a specific protein marker for T-tubule membranes. Data points represent the mean ± S.E.M. of 20–24 determinations carried out in three different SR fraction preparations. Results are consistent with the lack of difference in charge movement and intracellular Ca^{2+} release between JP45KO and WT mice at 18 months.

3.3. Age-dependent JP45 expression in WT and SR protein composition in JPKO mice

We examined JP45 expression in 3–18 month-old WT mice. Adding a third time point (6 months) helped us to define a steady decline in protein expression from the early to late ages (Fig. 2A and B). We also analyzed the levels of specific molecules expressed in the SR membrane and lumen to determine whether an increase in any of them compensates for the lack of JP45 expression in JP45KO mice with aging. Figure 2C–D shows expression of the SR Ca^{2+} release channel RyR and sarcoplasmic/endoplasmic reticulum Ca^{2+} pump-1 and -2 (SERCA1/2). Protein expression was normalized to albumin levels. Albumin was selected as a reference because we did not observe a significant difference in its content in the isolated sarcotubular membrane fractions from JP45KO and WT mice (Delbono et al., 2007). We also examined sarcalumenin, a major luminal Ca^{2+}-binding protein that mediates ion shuttling in the longitudinal SR; calreticulin, a low-affinity, high-capacity Ca^{2+}-binding protein; and calsequestrin, an SR terminal cisternae Ca^{2+}-binding protein with significant influence on SR Ca^{2+} release. None of these proteins differed significantly in 12- (C) or 18- (D) month JP45KO mice. Thus, compensatory overexpression of the major triadic proteins as a result of JP45KO is unlikely, but we cannot rule out a role for minor triadic proteins (see Discussion).

3.4. Spontaneous and forced activity in JP45KO and WT mice

To determine whether sustained skeletal muscle contraction force in JP45KO mice improves whole body performance, we tested their spontaneous and forced activity compared with that of age-matched WT littermates. Figure 3A shows running distance over 10 sec. recorded from 5 P.M. to 5 A.M in JP45KO (triangles) and WT (squares) mice. In contrast to 3–4 months (Delbono et al., 2007) (A), total spontaneous running distance decreased approximately 70% in 12- (B) and 18- (C) month mice, with a negligible difference between types.

To measure physical performance and endurance independent of motivation, we examined forced mechanical activity in JP45KO and WT mice (Fig. 3D). After a training period, mice were subjected to the experimental running program described below (Methods). Young (2–3 month) WT mice tend to run longer than JP45KO, consistent with the weaker in vitro muscle contraction recorded in JP45KO. This trend is no longer apparent at 12–14 months and reversed at 18 months, when JP45KO mice run longer (15.9 ± 0.9 m/min) than WT mice (11.8 ± 0.6) ($P < 0.01$); while WT mice reach a pace of 18 m/min, JP45KO mice average 22 m/min. We conclude that the sustained charge movement, $Ca_V1.1$ expression, and in vitro contraction force recorded in JP45KO mice sustains their physical performance across ages.

3.5. Body weight, food intake, and high-fat diet

Similar spontaneous activity and age-dependent forced activity, maintained in JP45KO but declining in WT mice, prompted us to examine their body weight and food intake because calorie restriction has been reported to preserve skeletal muscle function in rodents (Mayhew et al., 1998). Figure 3E shows body weight recorded in JP45KO and WT mice at 3, 4, 12 and 18 months. JP45KO mice weigh significantly less than WT mice at all ages. Reduced food intake is explained by the fact that JP45KO mice ate significantly less than WT mice during 20 days of observation at 12 months (Fig. 3F) and 18 months (Fig. 3G) of age. The significant decrease in body weight in JP45KO compared with WT indicates that decreased food intake in the former starts at early ages.

A linear regression analysis examined the relationship between ECC measurements and food intake in 18-month-old JP45KO mice. A negative relationship was observed between specific tetanic force (Pearson correlation coefficient, $r = -0.443$) or maximal charge movement ($r=-0.563$) and foot intake, which further supports the concepts that endogenously determined restriction in food intake enhances specific force and $Ca_V1.1$ expression.

To further examine their eating habits, we exposed 5-week JP45KO and WT mice to a high-fat diet (D12492 rodent diet with 60 kcal% fat; Research Diets, New Brunswick, NJ) for 33 weeks. Initially, the increase in body weight was similar but differed significantly at week 15, indicating that JP45KO mice are less susceptible than WT to obesity, even when challenged by a high-fat diet (Fig. 3H). We applied the diet at this early age, rather than when JP45KO consume significantly less food than WT (12- or 18-month), based on previous observations that very young mice are more prone to develop obesity when offered a high-fat diet (Shi et al., 2004). This indicates that JP45KO exhibits less tendency to develop obesity than WT mice.

3.6. Muscle fiber-type composition

To determine whether sustained force in JP45KO mice results from changes in muscle fiber-type composition, we examined MHC isoforms in EDL and soleus muscles from 12- and 18-month JP45KO and WT mice (Fig. 4). All EDL fibers are type-II, and our immunostaining technique found no type-I fibers (Fig. 4A, B). Soleus muscles showed more fast-than slow-

twitch fibers at both ages. We found no significant difference in MHC I or MHC II between JP45KO and WT mice at 12 months (Fig. 4A, C), but at 18 months, fiber-type profile analysis showed increased slow- and decreased fast-twitch fibers (Fig. 4B, D). These results indicate that JP45KO does not prevent the typical switch in fiber-type profile reported for aging skeletal muscle (Larsson, 1995).

3.7. EDL and soleus muscle fiber size from JP45KO and WT mice

To examine whether age-dependent changes in fiber size influence muscle performance in vivo and in vitro, we analyzed the distribution in EDL and soleus fibers from 12- and 18-month JP45KO and WT mice (Fig. 4). EDL (E) and soleus (F) fiber diameter ranged from 15 to 75 μm and 25 to 75 μm, respectively, with more fibers at 55 μm for both muscles from 12-month mice. JP45KO and WT mice did not differ (G); the range of fiber diameters at both ages was similar. The higher percent of EDL (H) and soleus (I) fibers from 18-month mice was 40 and 45 μm, respectively. We detected no significant difference between 18-month JP45KO and WT mice (J). These results indicate that JP45KO does not affect age-related changes in fiber size distribution.

Figure 4 also shows soleus muscle fiber diameter distribution based on MHC composition in the mice at both ages. MHC I fibers ranged from 35 to 75 μm, with a maximum of 55 μm for WT and 40 μm for JP45KO mice at 12 months ($P < 0.05$) (K). This shift toward smaller fibers is also apparent at 12 months for MHCII (K), though not statistically significant. Similarly, type I (L) and II (N) fibers peak at 45 μm for 18-month JP45KO and WT mice, and no significant difference was observed at 12 months (N). At 18 months, for type II fibers in soleus muscle, the percent of 45 μm increased and 50 μm decreased. These results are unlikely to explain the sustained fiber force and endurance in aging JP45KO mice.

3.8. Insulin and leptin determinations

Insulin and leptin concentrations were determined in 4–24 month mice. Figure 5 shows individual determinations of leptin (A, C) or insulin (B, D) as a function of age (A, B) and mouse weight (C, D). Serum leptin but not insulin increases as a function of age and body weight. Leptin concentration, expressed as mean ± SEM, for all mice 11-month or older was: 11.7 ± 2.2 ng/ml (n = 8) and 13.6 ± 2.4 (n =10) for WT and JP45KO mice, respectively, while insulin was 2.8 ± 0.9 ng/ml (n = 10) and 3.2 ± 1.2 (n = 12). No statistically significant differences between JP45KO and WT were found. These results indicate that JP45 ablation does not modify leptin or insulin secretion with aging.

3.9. JP45 expression in the hippocampus and proposed model for hypothalamic neuropeptide network operation

A previous report supports the lack of JP45 expression in total microsomal and mRNA from the mouse brain (Anderson et al., 2003), however, we re-examined this tenet using immunocytochemistry based on the possibility JP45 expression may be restricted to small areas and/or below the level of immunodetection in the whole brain. Figure 6 illustrates JP45 expression in the hyppocampal nuclei of 3–4-month WT (A) and JP45KO (B) mice in brain coronal sections near the third ventricle. The dotted JP45 fluorescence pattern indicates intracellular and probably organelle-associated expression. The specificity of the signal was tested by omitting the JP45 primary antibody (C) or replacing it with rabbit IgG (D). These results support the concept that JP45 is expressed in the brain and may be associated with the food intake central circuitry. To examine whether JP45 ablation alters neuropeptide expression, we performed quantitative real-time PCR for neuropeptide-Y (NPY), agouti-related peptide (AgRP), pro-opiomelanocortin (POMC) (E), thyrotropin-releasing hormone (TRH), and corticotropin-releasing hormone (CRH) (F) in isolated arcuate (ARH) and paraventricular (PVN) hypothalamic nuclei and measured their

transcript. Significantly decreased neuropeptide-Y (NPY) and possibly agouti-related peptide (AgRP) but not pro-opiomelanocortin (POMC), were associated with increased thyrotropin-releasing hormone (TRH), and corticotropin-releasing hormone (CRH). We propose a model in which JP45 ablation reduces endoplasmic reticulum (ER) Ca^{2+} release and Ca^{2+} influx through voltage-gated Ca^{2+} channels, resulting in reduced NPY and AgRP but not POMC expression in ARH neurons, leading to increased TRH and CRH in PVN neurons, reduced food intake, and the lean JP45KO mouse phenotype (G).

4. DISCUSSION

This work's main conclusion is that at 12 and 18 months, in contrast to WT mice, forced running and in vitro contractility in JP45KO mice was similar to 3–4 month mice. This maintained in vivo and in vitro muscle performance was associated with stable $Ca_v1.1$ expression, charge movement, and SR Ca^{2+} release. JP45KO mice at 12 and 18 months exhibited the same level of ECU reported for 3–4-month mice (Delbono et al., 2007). Moreover, their preserved ECC was associated with significantly diminished food intake, body weight, less tendency to develop obesity when exposed to a high-fat diet, and ablation of JP45 expression in the brain. We propose that JP45 ablation impairs intracellular Ca^{2+}, resulting in selective NPY and AgRP expression in ARH neurons, reduced food intake, and the lean JP45KO mouse phenotype.

4.1. Sustained skeletal muscle performance with aging recorded in vivo and in vitro in JP45KO mice

Aging is characterized by reduced skeletal muscle mass and specific force in mammalian species, including humans (Delbono, 2011; Gonzalez et al., 2000a). EDL and soleus muscle twitch and absolute tetanic force are significantly reduced in 12-month JP45KO compared to WT mice. However, tetanic absolute and specific force in both EDL and soleus muscle, which differ significantly between JP45KO and WT mice at 3–4 months (Delbono et al., 2007), do not differ significantly at 12 and 18 months. Previous work from our and other laboratories showed a decrease in EDL, soleus (Gonzalez et al., 2000b), and FDB (González et al., 2003) muscle fiber specific force with aging and proposed ECU as the underlying mechanism. Other theories include contraction-induced injury and posttranslational modifications of contractile proteins . Although contraction-induced injury after lengthening contractions has been reported in humans and reproduced in animal models (Faulkner and Brooks, 1995), diminished specific force has been recorded in the absence of this stress (Gonzalez et al., 2000a; González et al., 2003), suggesting that other mechanisms must be operating as well. The lack of change in specific force in manually skinned mouse EDL fibers, where activation of $Ca_v1.1$/RyR coupling was bypassed, argues against the proposal that posttranslational modifications in aging muscle switch contractile proteins from strongly to weakly bound actomyosin (for a review see (Delbono, 2011).

The data reported here support the conclusion that contraction efficiency depends on ECC. $Ca_v1.1$ expression, which is significantly lower in muscles from JP45KO mice at 3–4 months, is no lower at 18 months. Intramembrane $Ca_v1.1$ charge movement and SR Ca^{2+} release do not differ significantly. The notion that $Ca_V1.1$ expression declines during old age is supported by several studies (Ryan et al., 2000) (O'Connell et al., 2008). Note that $Ca_V1.1$ mRNA does not decrease significantly with age (Zheng *et al.* 2001), implicating some other mechanism in the decline in its protein level. Previous work demonstrated that $Ca_V1.1$ expression also declines following endogenous overexpression of $Ca_V\beta^{1a}$ with aging (Taylor et al., 2009). Future studies should determine whether JP45KO alters β1a expression.

JP45 expression in wild-type mice with aging does not reduce food intake and body mass probably because it is reduced only 20% compared to complete protein ablation in the

JP45KO mouse. Progressive decrease in $Ca_v1.1$ expression in wild-type mice leads to reduced contraction force at 18 months, not before, probably due to a $Ca_v1.1$ and SR calcium release safety margin; that is, both must decline below certain critical values to result in depressed mechanical output.

Lack of changes in triadic proteins in 12- and 18-month JP45KO mice rules out a compensatory effect of major triadic protein overexpression with aging but not the contribution of other mechanisms involved in myofiber Ca^{2+} homeostasis, such as store-operated Ca^{2+} entry (SOCE) and excitation-coupled Ca^{2+} entry (ECCE) (Lyfenko and Dirksen, 2008). The role of other minor SR membrane components that modulate ECC in striated muscles, such as mitsugumin-29, SRP-27/TRIC-A, and junctate/humbug, in sustained muscle performance with age has not been investigated.

Sustained exercise on a treadmill requires the activation of a complex biological mechanism, including appropriate neural drive and preserved nerve-muscle integrity and transmission. Maintaining skeletal muscle strength is crucial to the sustained response to a forced exercise regime seen here. Resistance to fatigue in aging animals has been attributed to a switch from fast to slow fiber type (Larsson and Ansved, 1995). We found more type-I and fewer type-II fibers in the soleus muscle of JP45KO compared to WT mice at 18 months, which, together with sustained ECC, probably accounts for their more prolonged running time.

Finally, myofiber number and cross-sectional area are major determinants of skeletal muscle force. We recorded atrophy in soleus muscle fiber, which indicates that fiber crosssectional area did not contribute to the sustained in vitro force measures and treadmill running distance recorded in aging JP45KO mice.

4.2 Endogenously determined restriction in food intake offsets JP45KO-dependent ECU

In this work, both JP45KO and WT mice had access to food and water ad libitum. Unexpectedly, compared to WT mice, the JP45KO mice ate less when exposed to Prolab RMH 3000 and tended significantly less toward obesity when exposed to a high-fat diet. We propose that calorie restriction accounts for their sustained muscle force and response to highly demanding treadmill exercise by modulating $Ca_v1.1$ expression. Previous reports on skeletal muscle from aging rodents and rabbits show a marked decline in $Ca_v1.1$ expression (Renganathan et al., 1997a; Renganathan et al., 1997b; Ryan et al., 2002). Here, we recorded more sustained $Ca_v1.1$ expression in aging JP45KO than WT mice. Maximal binding capacity in both at 18 months was remarkably lower than in 3–4 month-old mice (Delbono et al., 2007); however, the decline was more marked for WT mice, leading to a nonsignificant difference in $Ca_v1.1$ expression compared with JP45KO mice. Calorie restriction prevents age-dependent decrease in skeletal muscle force (Mayhew et al., 1998) and $Ca_v1.1$ expression (Renganathan and Delbono, 1998), in addition to increase life span (Barzilai and Bartke, 2009). While the magnitude of restriction here (~20–25%) and in our previous work (40%) (Mayhew et al., 1998) differs, levels in this range have been reported to prevent age-associated tissue function decline and disease in the mouse and other species (for a review, see (Yu, 1999). Development was unaffected, as JP45KO mice did not seem to reduce their intake in the first weeks of life; no significant differences in body weight were detected.

Many calorie restriction regimes have been applied to rodents and monkeys (Yu, 1999). Human subjects are participating or have participated in approximately 84 clinical trials of dietary interventions (*ClinicalTrials.gov*). To our knowledge, this model of “endogenously determined” restriction of food intake is the first reported in the literature. Since spontaneous activity in JP45KO and WT mice is similar, energy expenditure does not account for differences in body weight.

4.3. The central nervous system and food intake in JP45KO mice

To explain calorie restriction in JP45KO mice, we looked for JP45 expression in areas of the brain associated with central regulation of food intake (Roche et al., 2008) in WT mice using a specific JP45 antibody (Anderson et al., 2006). We found that JP45 is expressed in periventricular hippocampus nuclei in WT but not JP45KO. These results are consistent with the detection of the JP45 transcript in 55-day-old C57BL/6J male mouse brain by situ hybridization (ISH) (Allen Institute for Brain Science; http://mouse.brain-map.org) (Lein et al., 2007).

To examine whether JP45KO alters neuropeptide expression, we analyzed their gene expression in the hypothalamus. Our model proposes that JP45 ablation results in reduced ER Ca^{2+} release and probably Ca^{2+} influx through voltage-gated Ca^{2+} channels (Yamamori et al., 2004), leading to reduced NPY and AgRP but not POMC expression in ARH neurons and increased TRH and CRH in PVN and reduced food intake. The mechanism by which JP45 differentially modulates neuropeptide gene expression may depend on the set of Ca^{2+} channels expressed in specific NPY or POMC-secreting neurons (Sun and Miller, 1999) or the distinct leptin-dependent modulation of intracellular signaling involved in gene expression (Wang et al., 2008).

We examined only male JP45KO and WT mice. To our knowledge, no gender difference in the response to various exogenous calorie restriction regimens has been reported; however, future studies on females and the effect of menopause are needed.

How restricted food intake regulates $Ca_v1.1$ expression is unknown. It has been associated with decreased growth hormone/insulin-like growth factor 1 (IGF-1 axis; (Chiba et al., 2007), but whether calorie restriction modifies IGF-1 concentration in skeletal muscle is unknown. The strong influence of IGF-1 auto/paracrine secretion on muscle protein synthesis and function has been shown (Florini et al., 1996). We reported that IGF-1 prevents age-dependent decline in $Ca_v1.1$ (Renganathan et al., 1998) by activating gene transcription (Wang et al., 1999b) and specifically regulates $Ca_v1.1$ transcription in muscle cells by acting on the cAMP-response element-binding (CREB) protein of the promoter (Zheng et al., 2002).

In conclusion, male JP45KO, in contrast to WT mice, sustains in vivo and in vitro skeletal muscle force as they age. At 3–4 months, perhaps earlier, they restrict their food intake even when offered a high-fat diet, resulting in significantly lower body weight than WT, which may account for their functional advantage. JP45 is involved in NPY and AgRP expression in the nucleus arcuate of the hypothalamus, which regulates food intake by means of regulating neuropeptides expressed in paraventricular and lateral nuclei neurons (Fig. 7).

Acknowledgments

This study was supported by grants from the National Institutes of Health/National Institute on Aging (AG07157 and AG15820) to Osvaldo Delbono and the Wake Forest University Claude D. Pepper Older Americans Independence Center (P30-AG21332). Grants from the Association Française Contre les Myopathie AFM and Progetti di Ricerca di Interesse Nazionale PRIN to Francesco Zorzato also funded this project. We thank Jackson Taylor for performing brain and spinal cord immunoblots and Alexander Birbrair for helping with mouse perfusion.

Abbreviations

ECU	excitation-contraction uncoupling
JP45	45kDa junctional protein

$Ca_v1.1$	voltage-gated calcium channel-skeletal muscle isoform
ER	endoplasmic reticulum
SR	sarcoplasmic reticulum
DHPR	dihydropyridine receptor
RyR	ryanodine receptor
NPY	neuropeptide-Y
AgRP	agouti-related peptide
POMC	proopiomelanocortin
TRH	thyrotropin-releasing hormone
CRH	corticotropin-releasing hormone
PVN	paraventricular nucleus
EDL	extensor digitorum longus
FDB	flexor digitorum brevis
Q	charge movement

References

Delbono O, Xia J, Treves S, Wang ZM, Jimenez-Moreno R, Payne AM, Messi ML, Briguet A, Schaerer F, Nishi M, Takeshima H, Zorzato F. Loss of skeletal muscle strength by ablation of the sarcoplasmic reticulum protein JP45. Proc Natl Acad Sci U S A. 2007; 104:20108–20113. [PubMed: 18077436]

Melzer W, Herrmann-Frank A, Luttgau HC. The role of Ca2+ ions in excitationcontraction coupling of skeletal muscle fibres. Biochimica et Biophysica Acta. 1995; 1241:59–116. [PubMed: 7742348]

Catterall WA, Goldin AL, Waxman SG. International Union of Pharmacology. XLVII. Nomenclature and structure-function relationships of voltage-gated sodium channels. Pharmacol Rev. 2005; 57:397–409. [PubMed: 16382098]

Catterall WA. Structure and function of voltage-gated ion channels. Annual Review of Biochemistry. 1995; 64:493–531.

Gonzalez E, Messi ML, Delbono O. The specific force of single intact extensor digitorum longus and soleus mouse muscle fibers declines with aging. J Membr Biol. 2000a; 178:175–83. [PubMed: 11148759]

Jimenez-Moreno R, Wang ZM, Gerring R, Delbono O. Sarcoplasmic reticulum Ca2+ release declines in muscle fibers from aging mice. Biophys J. 2008; 94:3178–3188. [PubMed: 18178643]

Renganathan M, Messi ML, Delbono O. Dihydropyridine receptor-ryanodine receptor uncoupling in aged skeletal muscle. Journal of Membrane Biology. 1997a; 157:247–53. [PubMed: 9178612]

Taylor JR, Zheng Z, Wang ZM, Payne AM, Messi ML, Delbono O. Increased CaVbeta1A expression with aging contributes to skeletal muscle weakness. Aging Cell. 2009; 8:584–94. [PubMed: 19663902]

Anderson AA, Altafaj X, Zheng Z, Wang ZM, Delbono O, Ronjat M, Treves S, Zorzato F. The junctional SR protein JP-45 affects the functional expression of the voltage-dependent Ca2+ channel Cav1.1. J Cell Sci. 2006; 119:2145–55. [PubMed: 16638807]

Wang ZM, Messi ML, Delbono O. L-type Ca2+ channel charge movement and intracellular Ca2+ in skeletal muscle fibers from aging mice. Biophysical Journal. 2000; 78:1947–1954. [PubMed: 10733973]

Mayhew M, Renganathan M, Delbono O. Effectiveness of caloric restriction in preventing age-related changes in rat skeletal muscle. Biochemical & Biophysical Research Communications. 1998; 251:95–9. [PubMed: 9790913]

Marzetti E, Lawler JM, Hiona A, Manini T, Seo AY, Leeuwenburgh C. Modulation of age-induced apoptotic signaling and cellular remodeling by exercise and calorie restriction in skeletal muscle. Free Radic Biol Med. 2008; 44:160–8. [PubMed: 18191752]

Sakuma K, Yamaguchi A. Molecular mechanisms in aging and current strategies to counteract sarcopenia. Curr Aging Sci. 2010; 3:90–101. [PubMed: 20158492]

Wang ZM, Messi ML, Delbono O. Patch-clamp recording of charge movement, Ca2+ current and Ca2+ transients in adult skeletal muscle fibers. Biophysical Journal. 1999a; 77:2709–2716. [PubMed: 10545370]

Adams BA, Tanabe T, Mikami A, Numa S, Beam KG. Intramembrane charge movement restored in dysgenic skeletal muscle by injection of dihydropyridine receptor cDNAs. Nature. 1990; 346:569–72. [PubMed: 2165571]

Hamill OP, Marty A, Neher E, Sakmann B, Sigworth FJ. Improved patch-clamp techniques for high-resolution current recording from cells and cell-free patches. Pflugers Arch. 1981; 391:85–100. [PubMed: 6270629]

Delbono O, Renganathan M, Messi ML. Regulation of mouse skeletal muscle L-type Ca2+ channel by activation of the insulin-like growth factor-1 receptor. Journal of Neuroscience. 1997; 17:6918–28. [PubMed: 9278527]

Woods CE, Novo D, DiFranco M, Vergara JL. The action potential-evoked sarcoplasmic reticulum calcium release is impaired in mdx mouse muscle fibres. J Physiol. 2004; 557:59–75. [PubMed: 15004213]

Saito A, Seiler S, Chu A, Fleischer S. Preparation and morphology of sarcoplasmic reticulum terminal cisternae from rabbit skeletal muscle. J Cell Biol. 1984; 99:875–85. [PubMed: 6147356]

Anderson AA, Treves S, Biral D, Betto R, Sandona D, Ronjat M, Zorzato F. The novel skeletal muscle sarcoplasmic reticulum JP-45 protein. Molecular cloning, tissue distribution, developmental expression, and interaction with alpha 1.1 subunit of the voltage-gated calcium channel. J Biol Chem. 2003; 278:39987–92. [PubMed: 12871958]

Shi H, Cave B, Inouye K, Bjorbaek C, Flier JS. Overexpression of suppressor of cytokine signaling 3 in adipose tissue causes local but not systemic insulin resistance. Diabetes. 2006; 55:699–707. [PubMed: 16505233]

Hu W, Tian C, Li T, Yang M, Hou H, Shu Y. Distinct contributions of Nav1.6 and Nav1.2 in action potential initiation and backpropagation. Nat Neurosci. 2009; 12:996–1002. [PubMed: 19633666]

Xue B, Pulinilkunnil T, Murano I, Bence KK, He H, Minokoshi Y, Asakura K, Lee A, Haj F, Furukawa N, Catalano KJ, Delibegovic M, Balschi JA, Cinti S, Neel BG, Kahn BB. Neuronal protein tyrosine phosphatase 1B deficiency results in inhibition of hypothalamic AMPK and isoform-specific activation of AMPK in peripheral tissues. Mol Cell Biol. 2009; 29:4563–73. [PubMed: 19528236]

Shi H, Tzameli I, Bjorbaek C, Flier JS. Suppressor of cytokine signaling 3 is a physiological regulator of adipocyte insulin signaling. J Biol Chem. 2004; 279:34733–40. [PubMed: 15181014]

Larsson L. Motor units: remodeling in aged animals. Journals of Gerontology. Series A, Biological Sciences & Medical Sciences. 1995; 50:91–5.

Delbono, O. Excitation-Contraction Coupling Regulation in Aging Skeletal Muscle. In: Lynch, GS., editor. Sarcopenia-Age-Related Muscle Wasting and Weakness. Mechanisms and Treatment. Springer; Victoria: 2011. p. 113-134.

Gonzalez A, Kirsch WG, Shirokova N, Pizarro G, Brum G, Pessah IN, Stern MD, Cheng H, Rios E. Involvement of multiple intracellular release channels in calcium sparks of skeletal muscle. Proc Natl Acad Sci U S A. 2000b; 97:4380–5. [PubMed: 10759554]

González E, Messi ML, Zheng Z, Delbono O. Insulin-like growth factor-1 prevents age-related decrease in specific force and intracellular Ca2+ in single intact muscle fibres from transgenic mice. J Physiol. 2003; 552:833–44. [PubMed: 12937290]

Faulkner JA, Brooks SV. Muscle fatigue in old animals. Unique aspects of fatigue in elderly humans. Advances in Experimental Medicine & Biology. 1995; 384:471–80. [PubMed: 8585473]

Ryan M, Carlson BM, Ohlendieck K. Oligomeric status of the dihydropyridine receptor in aged skeletal muscle. Mol Cell Biol Res Commun. 2000; 4:224–9. [PubMed: 11409916]

O'Connell K, Gannon J, Doran P, Ohlendieck K. Reduced expression of sarcalumenin and related Ca2+-regulatory proteins in aged rat skeletal muscle. Exp Gerontol. 2008; 43:958–61. [PubMed: 18762239]

Lyfenko AD, Dirksen RT. Differential dependence of store-operated and excitationcoupled Ca2+ entry in skeletal muscle on STIM1 and Orai1. J Physiol. 2008 jphysiol.2008.160481.

Larsson L, Ansved T. Effects of ageing on the motor unit. Progress in Neurobiology. 1995; 45:397–458. [PubMed: 7617890]

Renganathan M, Messi ML, Schwartz R, Delbono O. Overexpression of hIGF-1 exclusively in skeletal muscle increases the number of dihydropyridine receptors in adult transgenic mice. FEBS Letters. 1997b; 417:13–6. [PubMed: 9395065]

Ryan AS, Dobrovolny CL, Smith GV, Silver KH, Macko RF. Hemiparetic muscle atrophy and increased intramuscular fat in stroke patients. Arch Phys Med Rehabil. 2002; 83:1703–7. [PubMed: 12474173]

Renganathan M, Delbono O. Caloric restriction prevents age-related decline in skeletal muscle dihydropyridine receptor and ryanodine receptor expression. FEBS Lett. 1998; 434:346–350. [PubMed: 9742952]

Barzilai N, Bartke A. Biological approaches to mechanistically understand the healthy life span extension achieved by calorie restriction and modulation of hormones. J Gerontol A Biol Sci Med Sci. 2009; 64:187–91. [PubMed: 19228789]

Yu, BP. Methods in Aging Research. 2. CRC Press; New York: 1999.

Roche JR, Blache D, Kay JK, Miller DR, Sheahan AJ, Miller DW. Neuroendocrine and physiological regulation of intake with particular reference to domesticated ruminant animals. Nutr Res Rev. 2008; 21:207–34. [PubMed: 19087372]

Lein ES, Hawrylycz MJ, Ao N, Ayres M, Bensinger A, Bernard A, Boe AF, Boguski MS, Brockway KS, Byrnes EJ, Chen L, Chen L, Chen TM, Chi Chin M, Chong J, Crook BE, Czaplinska A, Dang CN, Datta S, Dee NR, Desaki AL, Desta T, Diep E, Dolbeare TA, Donelan MJ, Dong HW, Dougherty JG, Duncan BJ, Ebbert AJ, Eichele G, Estin LK, Faber C, Facer BA, Fields R, Fischer SR, Fliss TP, Frensley C, Gates SN, Glattfelder KJ, Halverson KR, Hart MR, Hohmann JG, Howell MP, Jeung DP, Johnson RA, Karr PT, Kawal R, Kidney JM, Knapik RH, Kuan CL, Lake JH, Laramee AR, Larsen KD, Lau C, Lemon TA, Liang AJ, Liu Y, Luong LT, Michaels J, Morgan JJ, Morgan RJ, Mortrud MT, Mosqueda NF, Ng LL, Ng R, Orta GJ, Overly CC, Pak TH, Parry SE, Pathak SD, Pearson OC, Puchalski RB, Riley ZL, Rockett HR, Rowland SA, Royall JJ, Ruiz MJ, Sarno NR, Schaffnit K, Shapovalova NV, Sivisay T, Slaughterbeck CR, Smith SC, Smith KA, Smith BI, Sodt AJ, Stewart NN, Stumpf KR, Sunkin SM, Sutram M, Tam A, Teemer CD, Thaller C, Thompson CL, Varnam LR, Visel A, Whitlock RM, Wohnoutka PE, Wolkey CK, Wong VY, Wood M, Yaylaoglu MB, Young RC, Youngstrom BL, Feng Yuan X, Zhang B, Zwingman TA, Jones AR. Genome-wide atlas of gene expression in the adult mouse brain. Nature. 2007; 445:168–176. [PubMed: 17151600]

Yamamori E, Iwasaki Y, Oki Y, Yoshida M, Asai M, Kambayashii M, Oiso Y, Nakashima N. Possible involvement of ryanodine receptor-mediated intracellular calcium release in the effect of corticotropin-releasing factor on adrenocorticotropin secretion. Endocrinology. 2004; 145:36–8. [PubMed: 14592949]

Sun L, Miller RJ. Multiple neuropeptide Y receptors regulate K+ and Ca2+ channels in acutely isolated neurons from the rat arcuate nucleus. J Neurophysiol. 1999; 81:1391–403. [PubMed: 10085364]

Wang JH, Wang F, Yang MJ, Yu DF, Wu WN, Liu J, Ma LQ, Cai F, Chen JG. Leptin regulated calcium channels of neuropeptide Y and proopiomelanocortin neurons by activation of different signal pathways. Neuroscience. 2008; 156:89–98. [PubMed: 18588949]

Chiba T, Yamaza H, Shimokawa I. Role of insulin and growth hormone/insulin-like growth factor-I signaling in lifespan extension: rodent longevity models for studying aging and calorie restriction. Curr Genomics. 2007; 8:423–8. [PubMed: 19412415]

Florini JR, Ewton DZ, Coolican SA. Growth hormone and insulin growth factor system in myogenesis. Endocrine Review. 1996; 17:481–517.

Renganathan M, Messi ML, Delbono O. Overexpression of IGF-1 exclusively in skeletal muscle prevents age-related decline in the number of dihydropyridine receptors. Journal of Biological Chemistry. 1998; 273:28845–28851. [PubMed: 9786885]

Wang ZM, Messi ML, Renganathan M, Delbono O. Insulin-like growth factor-1 enhances rat skeletal muscle L-type Ca^{2+} channel function by activating gene expression. Journal of Physiology. 1999b; 516:331–341. [PubMed: 10087334]

Zheng Z, Wang ZM, Delbono O. Insulin-like growth factor-1 increases skeletal muscle DHPR alpha 1S transcriptional activity by acting on the cAMP-response element-binding protein element of the promoter region. Journal of Biological Chemistry. 2002; 277:50535–50542. [PubMed: 12407098]

- Aging JP45KO mice exhibited sustained excitation-contraction (EC) coupling.
- JP45 ablation impaired hypothalamic neuropeptide expression.
- Ablation of JP45 expression significantly diminished food intake and body weight.
- JP45KO resulted in endogenous caloric restriction, which prevented EC uncoupling.

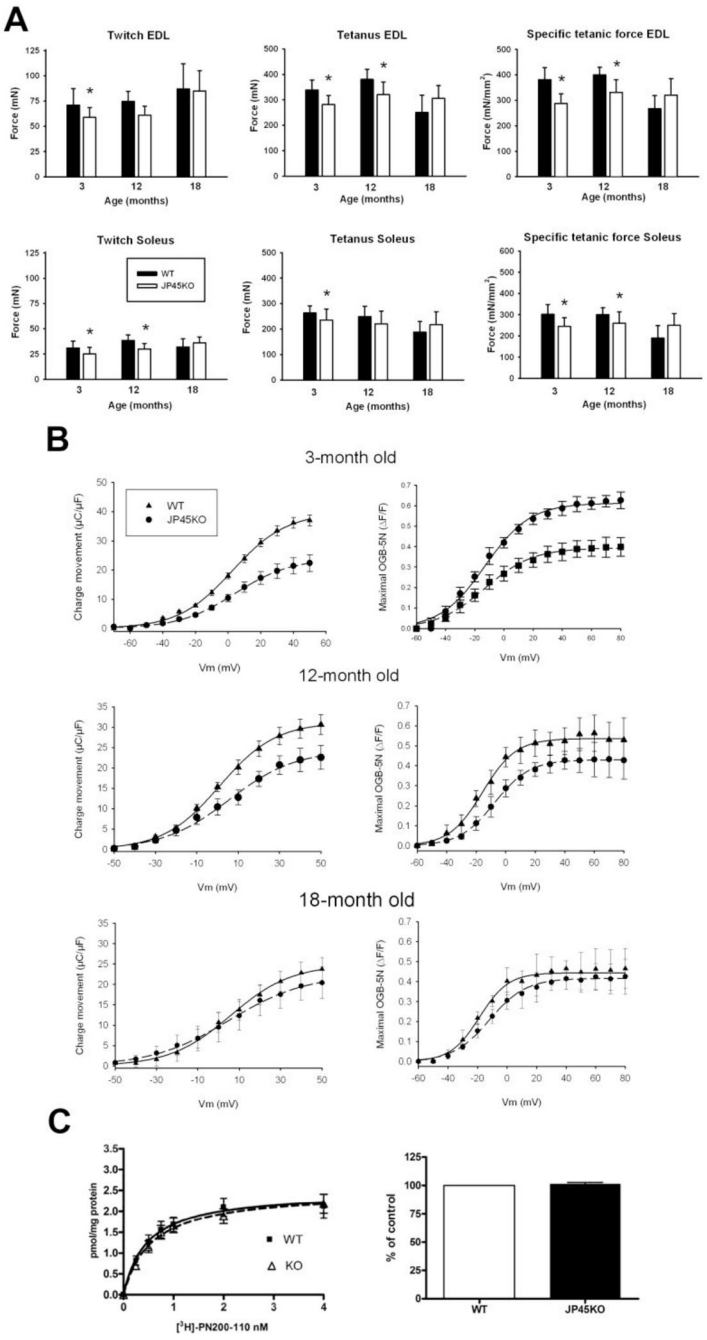

Figure 1. Skeletal muscle force, $Ca_V1.1$ charge movement and content in total SR membrane from JP45 KO and WT mice

A. Twitch, tetanic force, and specific force recorded in WT and JP45KO EDL and soleus muscles. The number of muscles tested was: EDL WT 3 [months] = 17; EWT12 = 14; EWT18=12; soleus [S] WT 3=15; SWT 12=13; SWT18 =9; EDL JP45KO [KO] 3=16; EKO12=14; EKO18=16; SKO3 =14; SKO12 =15; and SKO18=11. Data points are expressed as mean ± SD. *ANOVA test P <0.05. Data for 3-month-old WT and JP45KO mice are from (Delbono et al., 2007). **B**. $Ca_V1.1$ charge movement recorded after blocking the inward Ca^{2+} current. Data points were fitted to equation 1. Table 2 shows bestfitting parameters. **C.** [^{3}H]-PN200-110 binding assay. R1 fraction proteins from 18-month JP45KO

and WT mice were separated by 7.5% PAGE, blotted, and stained with a peroxidaseconjugated antibody against albumin (see Methods). Albumin content was measured by densitometry of the protein band. Data of 20–24 determinations carried out in three different total SR fraction preparations. Data for 3-month-old mice are from (Delbono et al., 2007). Data points represent mean ± S.E.M.

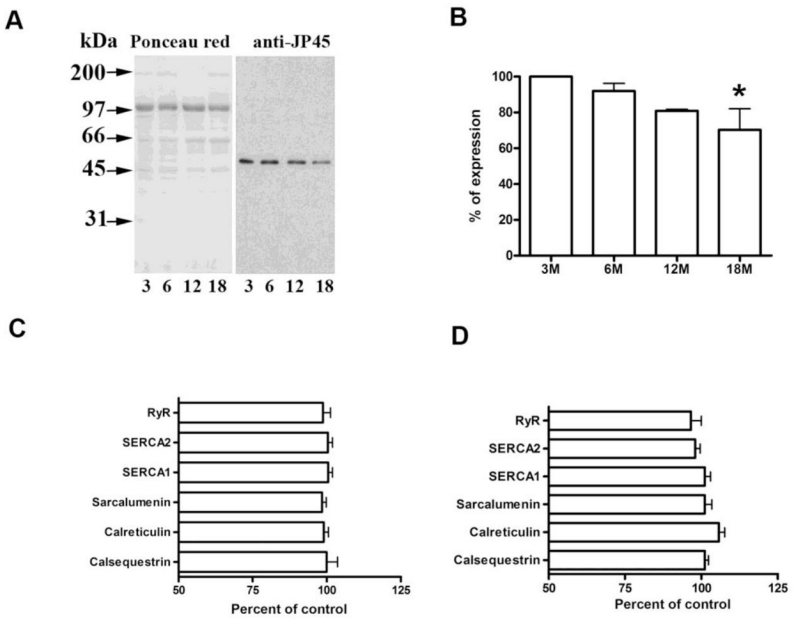

Figure 2. Age-dependent JP45 expression in WT and SR protein composition in JPKO mice

A. Western blot analysis of JP45 expression in microsomes from 3, 6, 12, and 18 monthold WT mice. **B**. JP45 expression at 6–18 months is represented as a percent at 3 months (n = 3). The asterisk indicates a statistically significant difference at 18 compared with 3 month-old mice ($p < 0.05$). Immunoblot analysis of SR fraction protein expression in 12- (**C**) and 18- (**D**) month JP45KO mice. Total SR (15μg) was separated on SDS gel and transferred to nitrocellulose membrane (n = 12–14 determinations in 2–3 SR membrane preparations). Data are expressed as a percent of albumin expression. Data for 3-month-old mice are from (Delbono et al., 2007). Values represent mean ± S.E.M.

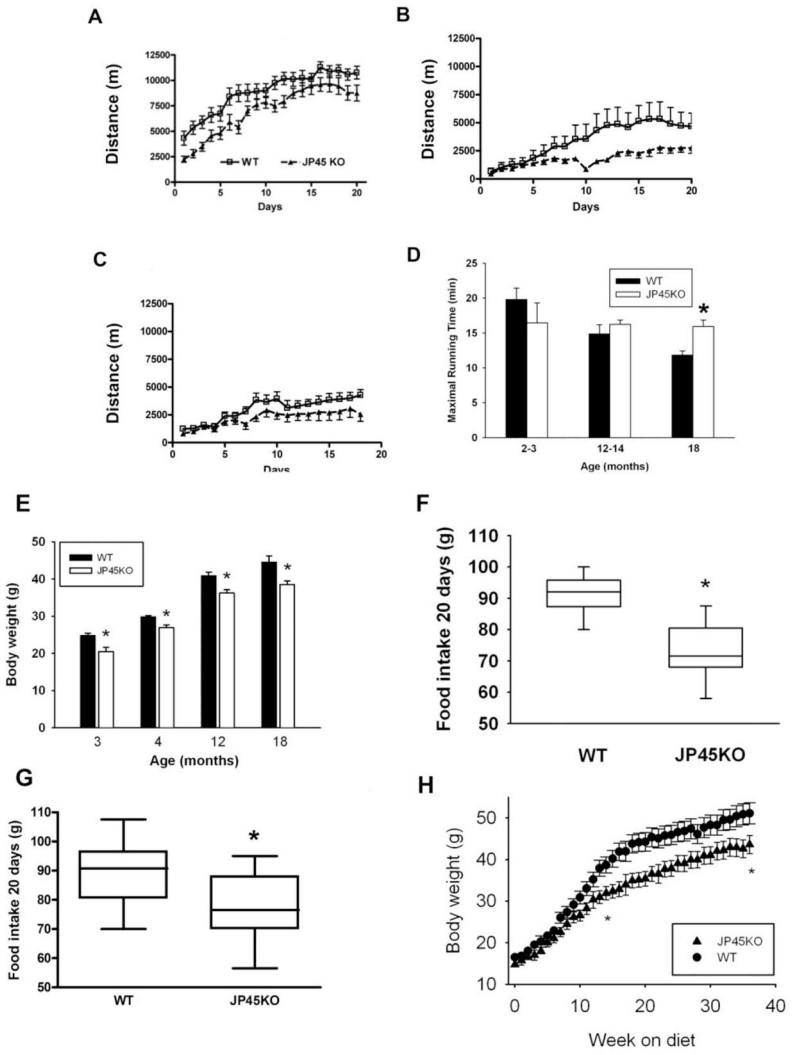

Figure 3. Spontaneous and forced activity, body weight and food intake in JP45KO and WT mice

Dark phase (5 P.M.-5 A.M.) running distance assessed in 3- (**A**), 12- (**B**) and 18- (**C**) month JP45KO (triangles) and WT (squares) mice, housed and equipped individually. Speed events represent the running distance over 10 sec. Data points from 3 (n = 12–14), 12 (n = 7–8) and 18 (n = 9–10) month-old mice. **D**. Maximal running time was measured using a forced treadmill. Data are compared with the 2–3-month-old mouse cohort. Data are mean ± S.E.M. for 2–3 (n= 6), 12–14 (n=6), and 18 (n=5) month-old mice. **E.** Body weight recorded in 3-month WT (n = 11) and JP45KO (n = 12); 4-month WT (n = 13) and JP45KO (n = 15); 12-month WT (n = 30) and JP45KO (n = 11) mice; and 18-month WT (n = 9) and JP45KO (n = 16) mice. *ANOVA test $P < 0.05$. **F**. Food consumed over a 20-day period by 13 JP45KO and 14 WT mice at 12 months of age. * $p< 0.05$. **G.** Food consumed over a 20-day period by 10 JP45KO and 10 WT mice at 18 months of age. * $p< 0.05$. **H.** Mouse body weight recorded at 5 weeks and for the next 33 weeks. Data points represent mean ± S.E.M of 6 JP45KO and 5 WT mice. Differences between asterisks are statistically significant.

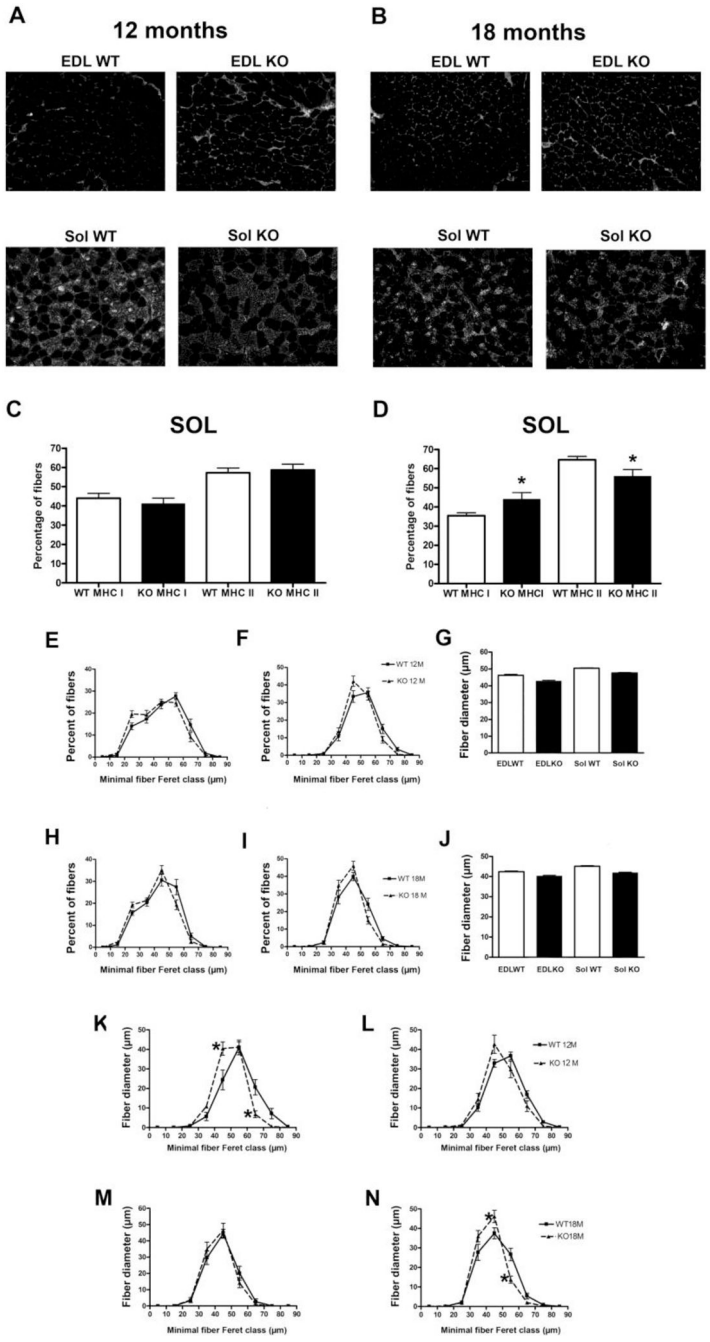

Figure 4. Fiber-type composition and fiber size in EDL and soleus muscle, and MHC fiber size distribution in soleus muscle from JP45 KO and WT mice

Myosin-heavy chain I (MHCI) composition in EDL and soleus muscles from (**A, C**) 12- and (**B, D**) 18-month-old mice. Fiber-type composition determined by myosin-heavy chain (MHC) immunocytochemistry in E[DL] WT 12 [months]= 4; EWT18 = 4; S[oleus]WT12 = 4; SWT18 = 4; E[JP45]KO12 = 4; EKO18 = 4; SKO12 = 4; and SKO18 = 4. Asterisks indicate statistically significant differences between JP45KO and WT mice ($P < 0.05$). EDL (**E**) and soleus (**F**) fiber size distribution and average minimal fiber Feret (**G**) in 12-month JP45KO and WT mice. EDL (**H**) and soleus (**I**) fiber size distribution and average minimal fiber Feret (**J**) in 18-month JP45KO and WT mice. The number of fibers analyzed was:

EWT12 = 1026; EKO12 = 1213; SWT12 = 869; SKO12 = 844; EWT18 = 1372; EKO18 = 1460; SWT18 = 1171; and SKO18 = 1377. MHC I distribution in (**K**) 12- and (**C**) 18-month JP45KO and WT mice and MHC II distribution in (**L**) 12- and (**D**) 18-month JP45KO and WT mice. For 12-month WT and JP45KO mice, the number of MHC I fibers studied was 376 and 220, respectively (**A**); MHC II fibers, 493 and 319, respectively (**B**). For 18-month WT and JP45KO mice, the number of MHC I fibers was 417 and 594, respectively (**M**); MHC II, 759 and 778, respectively (**N**). Values represent mean ± S.E.M.

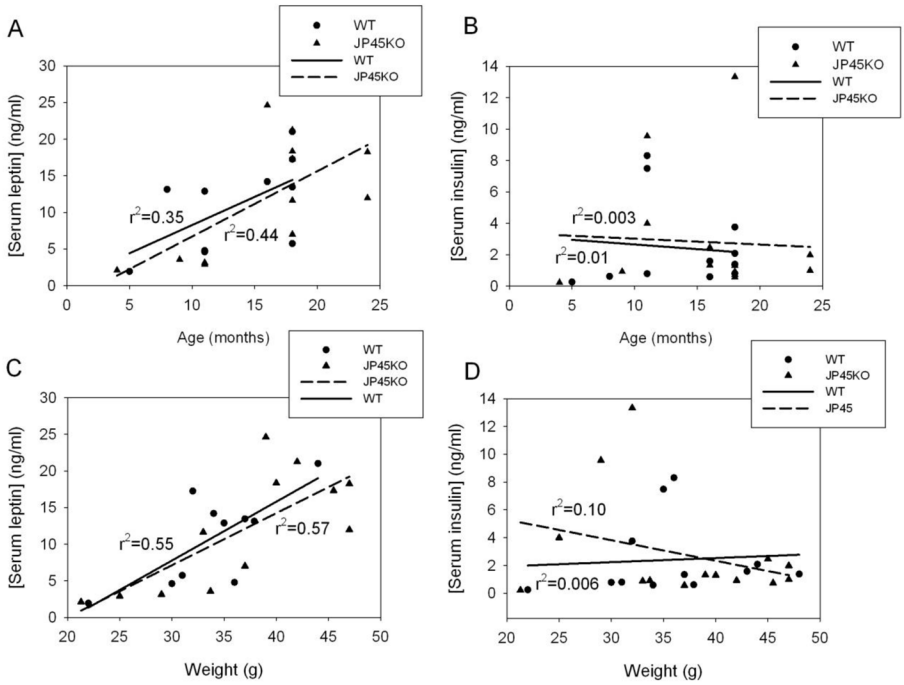

Figure 5. Serum leptin and insulin concentration in JP45KO and WT mice

Individual serum leptin concentration determination as a function of age (4–24 months) (A) or mouse weight (C). Serum insulin concentration as a function of age (B) or weight (D). Linear regression lines for JP45KO and WT mice are superimposed.

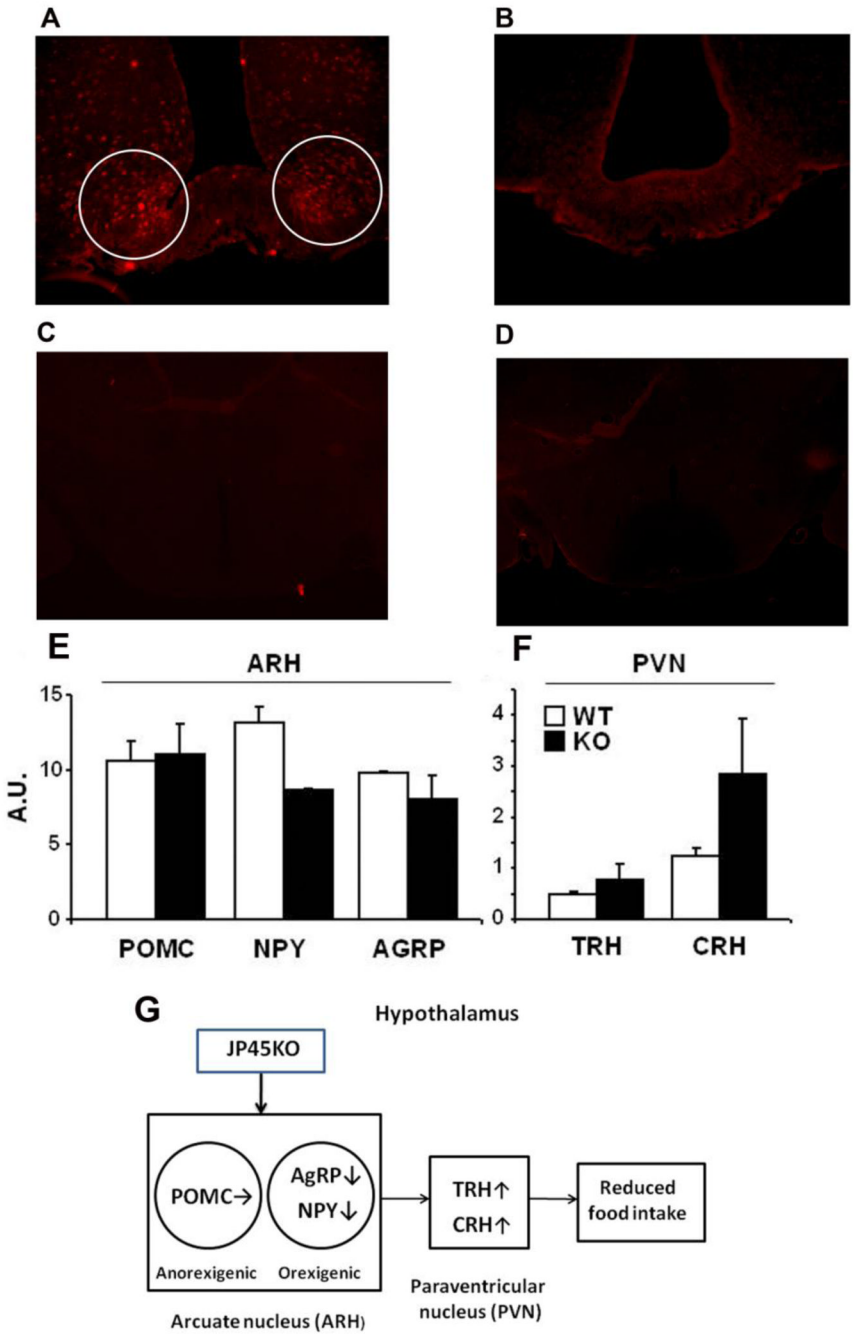

Figure 6. JP45 expression in hipothalamus, effect of JP45 ablation on hypothalamic neuropeptide expression and proposed model for neuropeptide network operation in JP45KO mice

Brain coronal sections showing JP45 expression in the arcuate nucleus of the hypothalamus of a WT mouse (**A**) and JP45KO mouse (**B**). Whole WT brain coronal sections in which the JP45 primary antibody was omitted (**C**) or replaced by rabbit IgG (**D**). Images are representative of brains from JP45KO (n = 3) and WT (n = 3) mice. (**E**) Expression of POMC, NPY and AGRP in arcuate hypothalamus (ARH). (**F**) Expression of TRH and CRH in paraventricular hypothalamus (PVN). Dissection of hypothalamic regions and measurement of gene expression have been described in Materials and Methods. Gene

expression was normalized to 18S ribosomal RNA level. Data are expressed as mean ± S.E.M. **G.** JP45KO leads to decreased neuropeptide-Y (NPY) and agouti-related peptide (AgRP) but not proopiomelanocortin (POMC) secretion, which results in increased thyrotropin-releasing hormone (TRH) and corticotropin-releasing hormone (CRH) secretion in the paraventricular nucleus and reduced food intake.

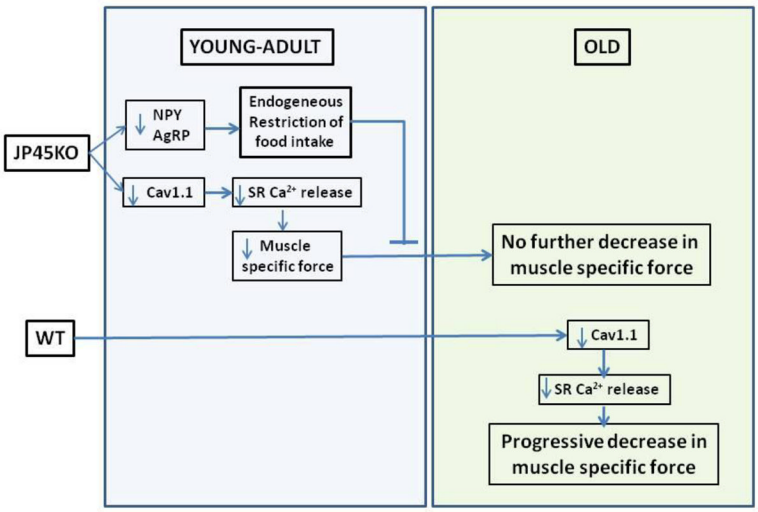

Figure 7. Time course of excitation-contraction uncoupling and endogenous caloric restriction in JP45KO and WT mice

Table 1

Neurotransmitter	Primers
Agouti Related Protein (AGRP)	5′-GCGGAGGTGCTAGATCCA-3′ (forward) 5′-AGGACTCGTGCAGCCTTA-3′ (reverse) 5′-CGAGTCTCGTTCTCCGCG-3′ (probe)
Neuropeptide-Y (NPY)	5′-CTCCGCTCTGCGACACTAC-3′ (f) 5′-AATCAGTGTCTCAGGGCT-3′ (r) 5′-CAATCTCATCACCAGACAG-3′ (p)
Pro-opiomelanocortin (POMC)	5′-ACCTCACCACGGAGAGCA-3′ (f) 5′-GCGAGAGGTCGAGTTTGC-3′ (r) 5′-TGCTGGCTTGCATCCGGG-3′ (p)
Thyrotropin-Releasing Factor (TRH)	5′-CTCTTCTCTCTGACAGCCC-3′ (f) 5′-AGGCGTGGAAGAACCGTC-3′ (r) 5′-TCTCTCGCCCCTTCGACAC-3′ (p)
Corticotropin-Releasing Hormone (CRH)	5′-GGAGCCGCCCATCTCTCT-3′ (f) 5′-CCGGGCCATTTCCAAGAC-3′ (r) 5′-ATCTCACCTTCCACCTTCTGCGGGA-3′ (p)
Ribosomal 18S	5′-AGTCCCTGCCCTTTGTACACA-3′ (f) 5′-GATCCGAGGGCCTCACTAAAC-3′ (r) 5′-CGCCCGTCGCTACTACCGATTGG-3′ (p)

Table 2

Charge movement				Intracellular Ca^{2+}		
Mice	**Q_{max}, μC/μF**	**$V_{1/2Q}$, mV**	***K***	**$\Delta F/F_{max}$**	**$V_{1/2F}$, mV**	***K***
3-M WT (n = 15–17)*	30.5 ± 3.4	7.6 ± 0.92	14.2 ± 1.8	0.61 ± 0.08	12.9 ± 0.19	15.4 ± 1.8
3-M JP45KO (n = 16–20)*	17.8 ± 2.6#	6.4 ± 0.75	12.0 ± 1.5	0.39± 0.06#	13.0 ± 0.15	16.3 ± 1.9
12-M JP45KO (n = 10)	24.4 ± 0.8	5.6 ± 1.7	16 ± 1.2	0.43 ± 0.03	7.5 ± 0.51	11.9 ± 0.44
12-M WT (n = 11)	31.2 ±0.5#	1.1 ± 1.8	13.6 ± 1.6	0.54 ± 0.06	15.7 ± 0.9	11.3 ± 0.75
18-M JP45KO (n = 12)	24.9 ± 0.6	5.9 ± 1.1	14.7 ± 0.8	0.42 ± 0.05	6.9 ± 0.9	12.3 ± 0.74
18-M WT (n = 14)	22.4 ± 0.5	5.1 ± 1.3	8.6 ± 0.8	0.44 ± 0.07	7.6 ± 1.2	9.8 ± 1.0

Values are mean ± SEM. "*n*" indicates the number of fibers.

# $P < 0.05$ statistically significant difference between WT and JP45KO mice.

* Data from ref. (Delbono et al., 2007).